Overview of mercury radionuclides and nuclear model calculations of $^{195}Hg^{m,g}$ and $^{197}Hg^{m,g}$ to evaluate experimental cross section data

M. Sadeghi,[1,*] M. Bakhtiari,[2,*] M. K. Bakht,[3,*] M. Anjomrouz,[3] and L. Mokhtari[4]

[1]*Agricultural, Medical and Industrial Research School, Nuclear Science and Technology Research Institute. P.O. Box 31485/498, Karaj, Iran*

[2]*Department of Physics, Persian Gulf University, Bushehr, Iran*

[3]*Department of Medical Radiation Engineering, Science and Research Branch, Islamic Azad University, Tehran, Iran*

[4]*Physics Faculty, University of Zanjan, Zanjan, Iran*

(Received 2 November 2011; published 13 March 2012)

Theoretical studies of isomers through nuclear reaction model calculations significantly assist the estimation of the different experimental data reported from different databases. In this paper, the production methods and the applications of mercury radionuclides are reviewed with special attention to the feasibility of the cyclotron production of mercury radionuclides, including $^{195}Hg^{m,g}$ and $^{197}Hg^{m,g}$. First, TALYS and EMPIRE codes were employed to illustrate the formation of both the isomeric and the ground states of the mercury radionuclides. Then the excitation function was calculated via a variety of nuclear processes using the codes and the data taken from the TENDL database. Then we compared the data with the reported experimental measurement. The mercury radionuclide production yield was evaluated with concentration on the excitation function calculations and the stopping powers of the projectiles in the targets. Last, the $^{197}Au(d,2n)$ and $^{197}Au(p,3n)$ reactions were selected as the best reactions to produce $^{197}Hg^{m,g}$ and $^{195}Hg^{m,g}$, respectively.

DOI: 10.1103/PhysRevC.85.034605 PACS number(s): 21.60.−n, 24.10.−i, 27.80.+w, 87.80.−y

I. INTRODUCTION

Radioisotopes play a significant role in life-science research, particularly in the pharmaceutical sciences [1,2]. The accelerator-produced isomers are broadly used in diagnostic medical applications [3,4]. Neves *et al*. [5] proposed $^{197}Hg^{m,g}$ as the new potential candidates for therapy. In medicine, the radioactive $^{197}Hg^{m,g}$ isomers have a low radiotoxicity, whereas all other mercury isotopes seem to have higher medical risks [6]. In addition, the radionuclide ^{203}Hg has many applications in monitoring the distribution and the accumulation of mercury in different parts of the body [7]. For instance, the effects of long-term daily mercury intake on urinary and fecal excretion, whole-body retention, blood concentration [8], and the maternal-fetal distribution of mercury released from dental amalgam fillings [9] were observed using mercuric chloride labeled with ^{203}Hg. Furthermore, $^{199}Hg^{m}$ is proposed as a potential radiopharmaceutical for lung-tumor imaging [7]. It should also be mentioned that the use of $^{195}Hg^{m}$ as a positron emitter radionuclide is debatable because the interaction between the positrons in the tissues results in the 511-keV annihilation photons; consequently, the annihilation photons increase the absorbed dose of the surrounding healthy tissues [5].

Additionally, mercury tracers are powerful tools to study mercury transformations in environmental systems. However, the most frequently used mercury radiotracer is ^{203}Hg [10], which is no longer regularly produced and is therefore now difficult to purchase. Therefore $^{197}Hg^{m}$ has been proposed as an alternative radiotracer [11].

The effects of isomeric impurities in medical radionuclides are evaluated in Refs. [12,13]. In fact, most of the special considerations in nuclear data studies are related to the production of diagnostic radioisotopes, such as the search for alternative production routes, the role of increasing the incident particle energy, and the detection of isomeric impurities [13]. Furthermore, theoretical studies of the isomers through nuclear reaction model calculations significantly assist the estimation of the different experimental data reported from different databases [14,15]. In this paper, we evaluate the cyclotron-production parameters of $^{195}Hg^{m,g}$ and $^{197}Hg^{m,g}$ via various codes for the nuclear model calculation of the cyclotron production of mercury radionuclides via different reactions; the maximum incident particle energy is 50 MeV, and the evaluation is performed as a part of the systematic studies on particle-induced activations on metal targets.

II. CALCULATIONS

A. Nuclear model calculations

The most up-to-date versions of the TALYS (version 1.26) and EMPIRE codes were employed to illustrate the formation of both the isomeric and the ground states of mercury radionuclides.

The nuclear reaction code system, EMPIRE, has been designed to perform nuclear reaction calculations over a wide range of energies and incident particles. The covered energy range is from resonance region (approximately keV) to several hundreds of MeV, and the projectile could be any nucleon or ion (including heavy ions) or a photon. EMPIRE is equipped with a complex system of codes to describe all the important nuclear reaction mechanisms [16]. The optical model and the direct reaction calculations were performed by the ECIS-03 code [17]. The optical model, discrete levels, and deformation parameters were retrieved from the Reference Input Parameter Library (RIPL)-2 library [18]. The direct-channel calculations

*Corresponding authors: msadeghi@nrcam.org; mahdi_6563@yahoo.com; mk.bakht@gmail.com

were performed by using the coupled-channel model or the distorted-wave Born approximation (DWBA) method. EMPIRE contains both the quantum-mechanical (MSD, MSC) and classical models (DEGAS, PCROSS, HMS) to describe preequilibrium reactions. The ORION and TRISTAN codes based on the work of Tamura *et al.* [19] are employed in EMPIRE to perform calculations for multistep direct (MSD) reactions. The multistep compound (MSC) calculations involve the approach of Nishioka, Verbaarschot, Weidenmüller and Yoshida (NVWY) theory [20], whereas γ-emission treatment is considered as in Ref. [21]. Both MSD and MSC are coupled together for quantum-mechanical treatment of preequilibrium processes. EMPIRE also contains the DEGAS module based on the exciton model for description of preequilibrium reactions with angular momentum conservation [22]. Preequilibrium emission can also be considered using the PCROSS code, which includes nucleon, γ, and cluster emissions. The option of EMPIRE-specific level densities was selected for all the calculations. An improved version of the Hauser-Feshbach theory was used for compound nucleus reactions. The width fluctuation corrections were based on the Hofmann, Richert, Tepel and Weidenmüller (HRTW) model [23]. The γ transitions were described by the Brink-Axel hypothesis [24,25].

Furthermore, the TALYS program [26] simulates the nuclear reactions that TALYS uses by default in the phenomenological optical model parameterizations for neutrons and protons on a nucleus-by-nucleus basis to obtain the transmission coefficients and the reaction cross sections [27]. If the potential is not available, TALYS automatically uses a global optical model. The TALYS code considers three types of reaction mechanisms: direct, preequilibrium, and compound reactions [28]. TALYS-1.2 is the latest version of the TALYS code, which has been released on the Internet. The important input parameters to the TALYS-1.26 computer program were (i) the simple folding approach parameterizations of Watanabe [29] optical model potentials for complex particles, (ii) the Constant temperature model (CTM) and Fermi gas models were used for level densities [30,31], (iii) the Hauser-Feshbach model [32] for equilibrium calculations, and (iv) the two-component exciton model by Kalbach [33] for preequilibrium calculations. All nuclei were considered nearly spherical in shape. Because we are involved in the development of this code, we have access to its most up-to-date version (TALYS-1.26), which is in the developmental state. Moreover, TALYS-based Evaluated Nuclear Data Library (TENDL) is a nuclear data library that provides the output of the TALYS nuclear model code system for direct use in both basic physics and applications with some modifications. The third version is TENDL-2010, which is based on both the default and the adjusted TALYS calculations and data from other sources [34]. Fortunately, EMPIRE-3 and TALYS-1.26 are able to calculate the excitation functions for the residual nuclide production, including the isomeric cross sections that are essential to calculate the excitation function of the mercury reactions.

B. Optical model parameters

The default optical model potentials (OMP) used in TALYS and EMPIRE were employed for the nuclear model calculations in the present study, except for the deuteron-induced reaction where we also used the potentials from the optical models proposed by Daehnick *et al.* [35], Bojowald *et al.* [36], Han *et al.* [37], and An *et al.* [38]. In general, Eq. (1) demonstrates the optical model potentials:

$$\begin{aligned} V(r) = &-V_R f(r, r_0, a_0) + i4a_I W_D \frac{d}{dr} f(r, r_I, a_I) \\ &- i W_s f(r, r_I, a_I) + V_{LS} \left(\frac{h}{m_\pi c}\right)^2 \\ &\times (\vec{L} \cdot \vec{S}) \frac{1}{r} \frac{d}{dr} f(r, r_{LS}, a_{LS}) + V_{\text{Coul}}, \end{aligned} \tag{1}$$

where the Woods-Saxon well f is given by

$$f(r, r_i, a_i) = \left[1 + \exp\left(\frac{(r - r_i A^{1/3})}{a_i}\right)\right]^{-1}. \tag{2}$$

A is the mass number, V_R and V_{LS} are the real potential and the real spin-orbit potential depths, respectively, W_D and W_s are the surface and the volume imaginary potential depths, respectively, r_i are the radii, and a_i are the diffuseness parameters.

In fact, for deuterons, tritons, ^{3}He, and α particles, TALYS uses a simplification of the folding approach of Watanabe [29]. For deuterons, the real central potential depth at the incident energy E is

$$V_V^{\text{deuteron}}(E) = V_V^{\text{neutron}}(E/2) + V_V^{\text{proton}}(E/2), \tag{3}$$

and similarly for W_V and W_D. For the spin-orbit potential depth, we have

$$V_{\text{SO}}^{\text{deuteron}}(E) = \left[V_{\text{SO}}^{\text{neutron}}(E) + V_{\text{SO}}^{\text{proton}}(E)\right]/2, \tag{4}$$

and similarly for W_{SO}. For the radius and the diffuseness parameter of the real central potential, we have

$$\begin{aligned} r_V^{\text{deuteron}} &= \left(r_V^{\text{neutron}} + r_V^{\text{proton}}\right)/2, \\ a_V^{\text{deuteron}} &= \left(a_V^{\text{neutron}} + a_V^{\text{proton}}\right)/2, \end{aligned} \tag{5}$$

and similarly for the geometry parameters of the other potentials, where V_V^{neutron}, V_V^{proton}, $V_{\text{SO}}^{\text{neutron}}$, $V_{\text{SO}}^{\text{proton}}$, r_V^{neutron}, r_V^{proton}, a_V^{neutron}, and a_V^{proton} are the global optical model parameters defined by Koning and Delaroche [27]. The global optical model for a neutron is

$$\begin{aligned} &V_V(E) = v_1^n\left[1 - v_2^n\left(E - E_f^n\right) + v_3^n\left(E - E_f^n\right)^2 - v_4^n\left(E - E_f^n\right)^3\right], \quad W_V(E) = w_1^n \frac{\left(E - E_f^n\right)^2}{\left(E - E_f^n\right)^2 + \left(w_2^n\right)^2}, \\ &r_V = 1.3039 - 0.4054\ \text{A}^{1/3}, \quad a_V = 0.6778 - 1.487 \times 10^{-4}\ \text{A}, \quad W_D(E) = d_1^n \frac{\left(E - E_f^n\right)^2}{\left(E - E_f^n\right)^2 + \left(d_3^n\right)^2} \exp\left[-d_2^n\left(E - E_f^n\right)\right], \end{aligned} \tag{6}$$

$$r_D = 1.3424 - 0.01585\ \mathrm{A}^{1/3}, \quad a_D = 0.5446 - 1.656 \times 10^{-4}\ \mathrm{A}, \quad V_{\mathrm{SO}} = v_{\mathrm{SO1}}^{n} \exp\left[- v_{\mathrm{SO2}}^{n}\left(E - E_f^n\right)\right],$$

$$W_{\mathrm{SO}}(E) = w_{\mathrm{SO1}}^{n} \frac{\left(E - E_f^n\right)^2}{\left(E - E_f^n\right)^2 + \left(w_{\mathrm{SO2}}^{n}\right)^2}, \quad r_{\mathrm{SO}} = 1.1854 - 0.647\ \mathrm{A}^{-1/3}, \quad a_{\mathrm{SO}} = 0.59,$$

and the global optical model for proton is

$$\begin{aligned} V_V(E) &= v_1^p\left[1 - v_2^p\left(E - E_f^p\right) + v_3^p\left(E - E_f^p\right)^2 - v_4^p\left(E - E_f^p\right)^3\right] + \overline{V_c} \cdot v_1^p\left[v_2^p - 2v_3^p\left(E - E_f^p\right) + 3v_4^p\left(E - E_f^p\right)^2\right], \\ W_V(E) &= w_1^p \frac{\left(E - E_f^p\right)^2}{\left(E - E_f^p\right)^2 + \left(w_2^p\right)^2}, \quad r_V = 1.3039 - 0.4054\ \mathrm{A}^{1/3}, \quad a_V = 0.6778 - 1.487 \times 10^{-4}\ \mathrm{A}, \end{aligned} \tag{7}$$

$$W_D(E) = d_1^p \frac{\left(E - E_f^p\right)^2}{\left(E - E_f^p\right)^2 + \left(d_3^p\right)^2} \exp\left[- d_2^p\left(E - E_f^p\right)\right], \quad r_D = 1.3424 - 0.01585\ \mathrm{A}^{1/3}, \quad a_D = 0.5187 + 5.205 \times 10^{-4}\ \mathrm{A},$$

$$V_{\mathrm{SO}} = v_{\mathrm{SO1}}^{p} \exp\left[- v_{\mathrm{SO2}}^{p}\left(E - E_f^p\right)\right], \quad W_{\mathrm{SO}}(E) = w_{\mathrm{SO1}}^{p} \frac{\left(E - E_f^p\right)^2}{\left(E - E_f^p\right)^2 + \left(w_{\mathrm{SO2}}^{p}\right)^2}, \quad r_{\mathrm{SO}} = 1.1854 - 0.647\ \mathrm{A}^{-1/3}, \tag{8}$$

$$a_{\mathrm{SO}} = 0.59, \quad r_C = 1.198 + 0.697\ \mathrm{A}^{-2/3} + 12.994\ \mathrm{A}^{-5/3}.$$

The above equations demonstrate that some of these parameters are mass dependent and some of them are energy dependent.

C. Calculation of theoretical yield

By growing the projectile energy, the beam current, and the time of bombardment, we increase the production yield. The production yield can be calculated as follows:

$$Y = \frac{N_L H}{M} I(1 - e^{-\lambda t}) \int_{E_1}^{E_2} \left(\frac{dE}{d(\rho x)}\right)^{-1} \delta(E) dE, \tag{9}$$

where Y is the activity (in Bq) of the product, N_L is Avogadro's number, H is the isotope abundance of the target nuclide, M is the mass number of the target element, $\sigma(E)$ is the cross section at energy E, I is the projectile current, $dE/d(\rho x)$ is the stopping power, λ is the decay constant of the product, and t is the time of irradiation [39]. The production yield of mercury radionuclides via several reactions was calculated using the Simpson numerical integral as in Eq. (9). According to the Stopping and Range of Ions in Matter (SRIM) code data, the finest required thicknesses of the targets for each reaction were calculated. The ranges of the projectiles in gold are given in Fig. 1. The physical thickness of the target layer was chosen to ensure that for a given beam-target angle geometry (90°), the incident beam exits the target layer with a predicted energy.

III. RESULTS AND DISCUSSION

A. Proton-induced reactions

1. *Excitation function of the* ^{197}Au*(p,3n)* ^{195}Hg^{m,g} *reaction*

The excitation function based on the TALYS-1.26 code calculation is shown in Fig. 2 at different decay channels

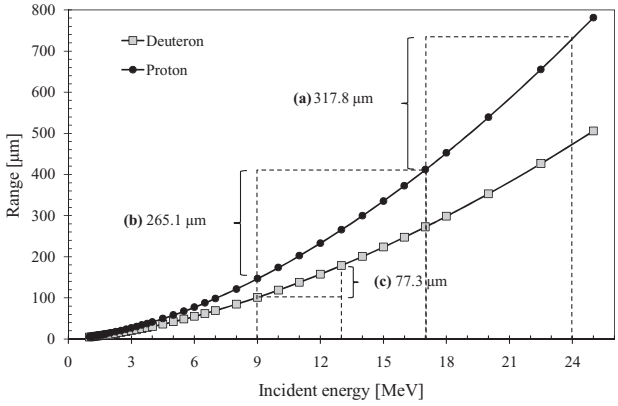

FIG. 1. Proton and deuteron range in gold (a) ^{197}Au$(p,3n)^{195}$Hg^{m,g}, (b) ^{197}Au$(p,2n)^{197}$Hg^{m,g}, and (c) ^{197}Au$(d,2n)^{197}$Hg^{m,g}.

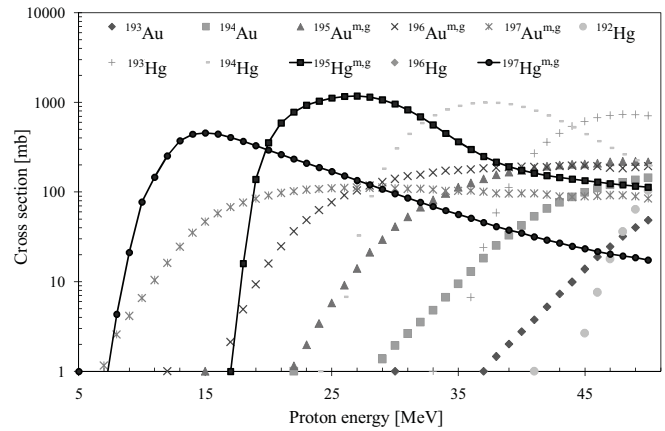

FIG. 2. TALYS-1.26 calculated excitation function of the ^{197}Au(p,x) reaction and the impurities produced from this reaction.

TABLE I. Mercury radionuclide production yield and target thickness for various reactions. N.A. means Not applicable.

Reaction	Energy range (MeV)	Theoretical yield, TALYS-1.26 code (MBq/μA h)	Theoretical yield, EMPIRE-3 code (MBq/μA h)	Theoretical yield, experimental data (MBq/μA h)	Q Value (MeV)	E threshold (MeV)	Target thickness (μm)
^{197}Au(p,3n)^{195}Hg^{m}	17–24	120.6	82.7	94.8 [40–42]	−17.2	17.3	317.8
^{197}Au(p,3n)^{195}Hg^{g}	17–24	349.8	228	256.3 [40,43]	−17	17.1	317.8
^{197}Au(p,3n)^{195}Hg$^{\text{total}}$	17–24	470.4	310.7	N.A.	−17	17.1	317.8
^{197}Au(p,n)^{197}Hg^{m}	9–17	17.8	27.7	19.5 [43–46]	−0.4	0.4	265.1
^{197}Au(p,n)^{197}Hg^{g}	9–17	7.7	11.7	6.7	0	0	265.1
^{197}Au(p,n)^{197}Hg$^{\text{total}}$	9–17	25.5	39.4	N.A.	−1.3	1.3	265.1
^{197}Au(d,2n)^{197}Hg^{m}	9–13	11.7	44	14.7 9 [47,51]	−3.6	3.6	77.3
^{197}Au(d,2n)^{197}Hg^{g}	9–13	4.3	11.2	15.1 [47]	−3.9	3.9	77.3
^{197}Au(d,2n)^{197}Hg$^{\text{total}}$	9–13	16	55.2	N.A.	−3.6	3.6	77.3

after the proton bombardment of natural gold (the isotopic abundance of ^{197}Au is 100%). The ^{197}Au(p,x) reaction leads to the formation of ^{197}Hg^{m,g}, ^{194}Hg, and gold impurities in the 17–35-MeV energy range. Chemical methods cannot be used to separate mercury contaminations but can be used to separate nonisotopic impurities. To eliminate the ^{194}Hg ($T_{1/2}$ = 520 years) impurity and to attain the full benefit energy, the 17–24-MeV energy range is considered in Table I. Unfortunately, ^{197}Hg^{m,g} ($T_{1/2}$ = 23.8 h, 64.14 h) cannot be removed by changing the range of the projectile energy; therefore, it is impossible to eliminate this isotopic impurity. At 27 MeV, the excitation function from TALYS-1.26 reaches the maximum cross section value of 1177 mb. Figure 3(a) shows the comparison between the isomer-state cross section values reported by Nagame *et al*. [40], Michel *et al*. [41], and Szelecsenyi *et al*. [42] and the results of the nuclear model calculations, which employ different theoretical calculations. In general, TALYS-1.26 and TENDL nuclear model calculations

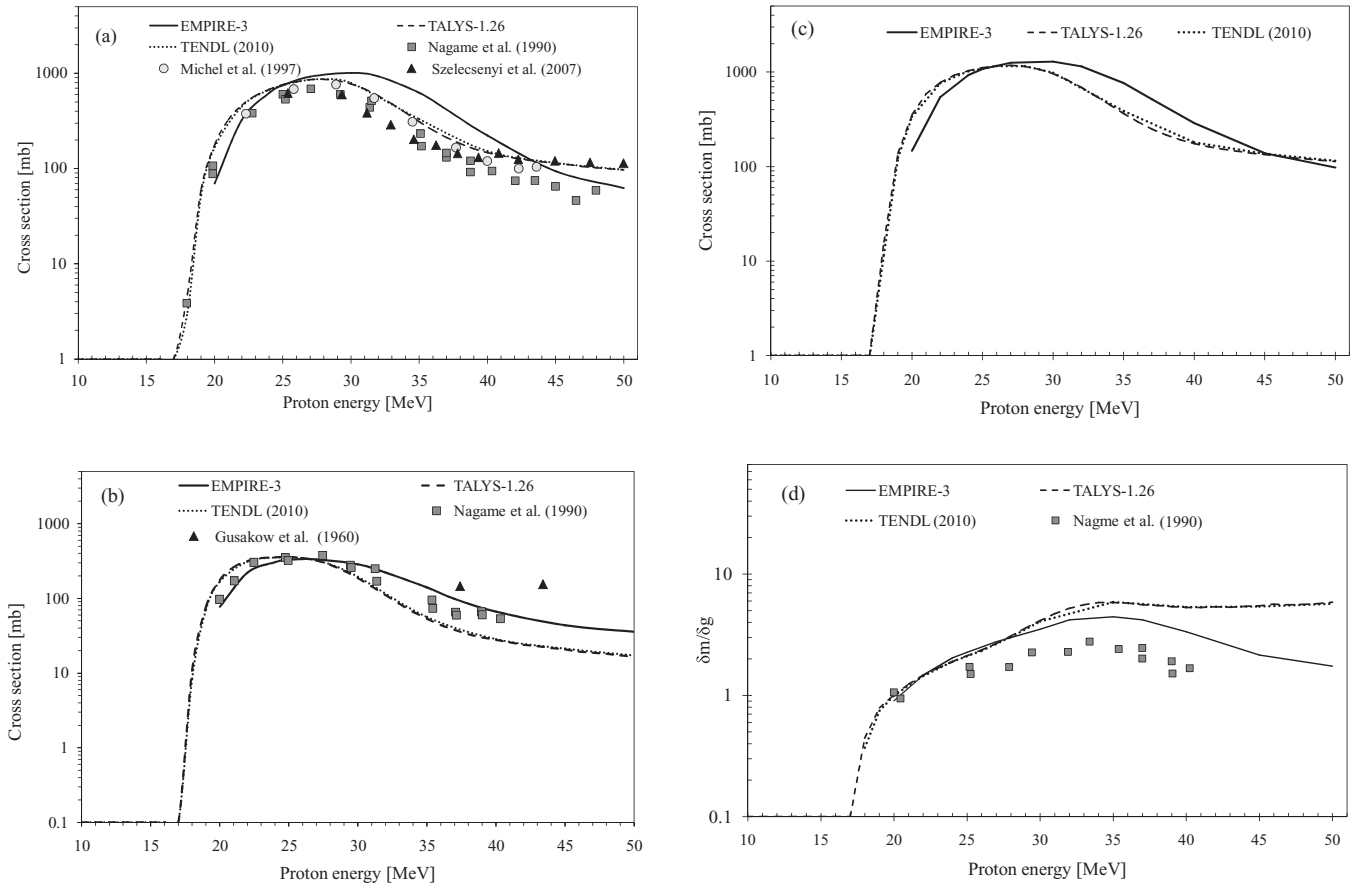

FIG. 3. Comparison between the experimental cross section data and the calculated excitation functions by TALYS-1.26, TENDL-2010, and EMPIRE-3 for the ^{197}Au(p,3n)^{195}Hg^{m,g} reaction (a) isomer-state population, (b) ground-state population, (c) total production cross section, and (d) isomer ratio in the ^{197}Au(p,3n)^{195}Hg^{m,g} process. The experimental data are from Refs. [40–43].

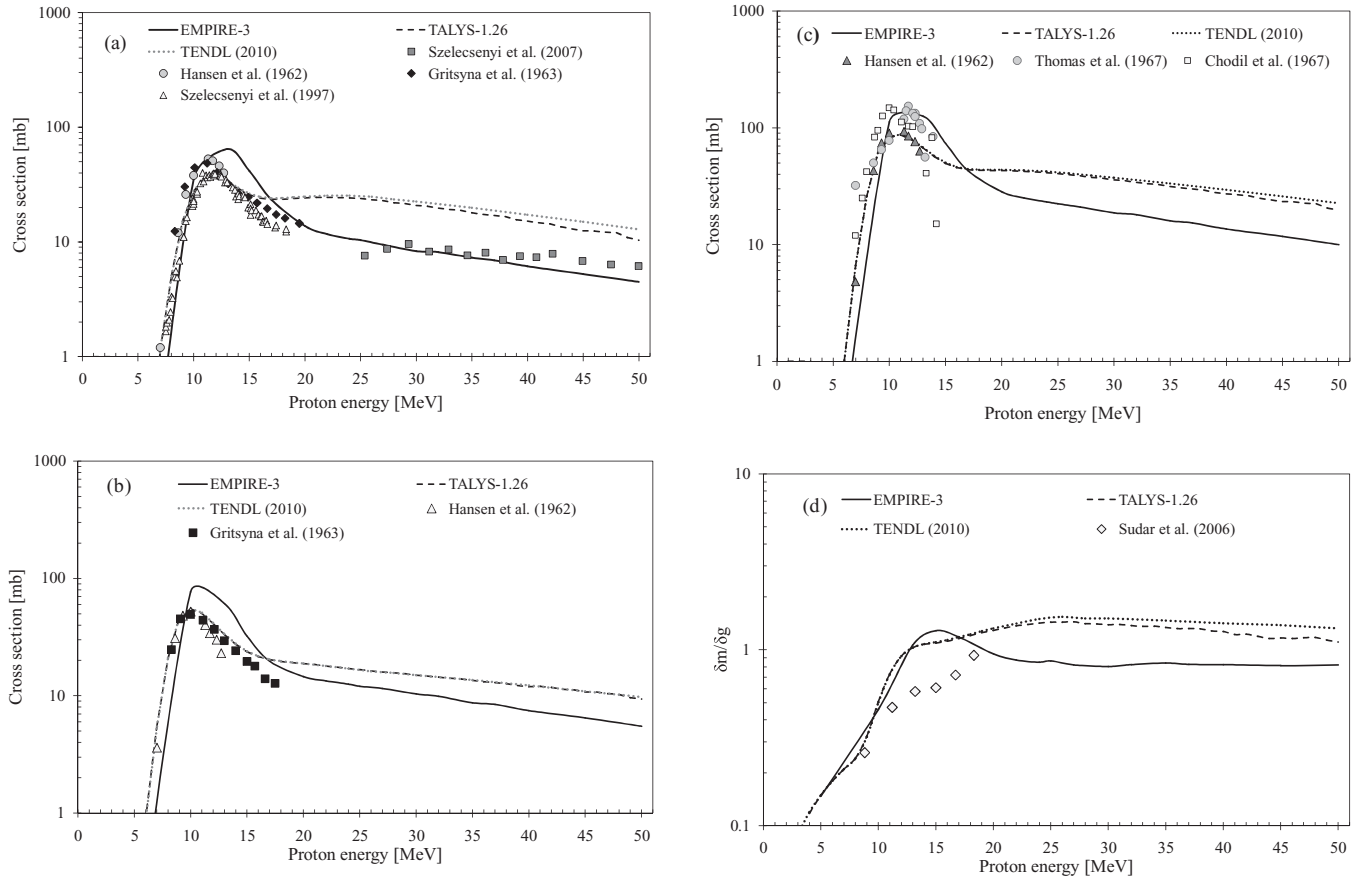

FIG. 4. Comparison between the experimental cross section data and the calculated excitation functions by TALYS-1.26, TENDL-2010, and EMPIRE-3 for the ^{197}Au$(p,n)^{197}$Hg^{m,g} reaction (a) isomer-state population, (b) ground-state population, (c) total production cross section, and (d) isomer ratio in the ^{197}Au$(p,n)^{197}$Hg^{m,g} process. The experimental data are from Refs. [42,44–49].

are in good agreement with most of the experimental cross section data. In the 28–42-MeV range, EMPIRE-3 overestimates the values to some extent. Alternatively, as shown in Fig. 3(b), the EMPIRE-3 calculated values are closer to the experimental measurements for ground-state cross sections, while TALYS-1.26 and TENDL overestimate the values above 30 MeV. More importantly, the isomer ratio in the ^{197}Au$(p,3n)^{195}$Hg^{m,g} process shows a high overestimation of the codes. Nonetheless, EMPIRE-3 illustrates the correct shape of the isomer ratio [Fig. 3(d)]. According to the SRIM code, the required target thickness should be 317.8 μm of gold.

2. *Excitation function of the* ^{197}Au$(p,n)^{197}$H^{m,g} *reaction*

According to Fig. 2, the ^{197}Au(p,x) reaction leads to the formation of ^{197}Hg^{m,g} and gold impurities in the 18–27 MeV energy range. While separation of isotopic contamination ^{197}Hg^{m,g} is not possible with chemical methods, the nonisotopic impurities can be separated using chemical methods. To eliminate the ^{195}Hg^{m,g} impurity and to reach the full benefit energy, the 9–17-MeV energy range is considered in Table I. At 28 MeV, the excitation function from TALYS-1.26 reaches the maximum cross section value of 865 mb. Figure 4(a) compares the experimental isomeric cross section values [42,46] with the results of the nuclear model calculations that utilize the theoretical calculations. Up to 15 MeV, the nuclear model calculation results are in good agreement with the experimental data. Above 25 MeV, EMPIRE-3 agrees with the experimental data and TALYS overestimates the values.

Figure 4(b) illustrates the comparison between the ground-state cross section values. Up to 16 MeV, the TALYS-1.26 results are in good agreement with the experimental data, but EMPIRE-3 overestimates the values. Above 17 MeV, the experimental data do not have the total and the ground-state cross sections. According to the SRIM code, the required target thickness should be 265.1 μm of gold.

B. Deuteron-induced reactions

1. *Excitation function of the* ^{197}Au$(d,4n)^{195}$Hg^{m,g} *reaction*

The excitation function calculated by TALYS-1.26 is shown in Fig. 5 at different decay channels after the deuteron bombardment of natural gold. At 33 MeV, the excitation function reaches the maximum cross section value of 639 mb. Unfortunately, in all energy regions of the ^{195}Hg^{m,g} production, a large quantity of stable ^{196}Hg impurity exists and cannot be

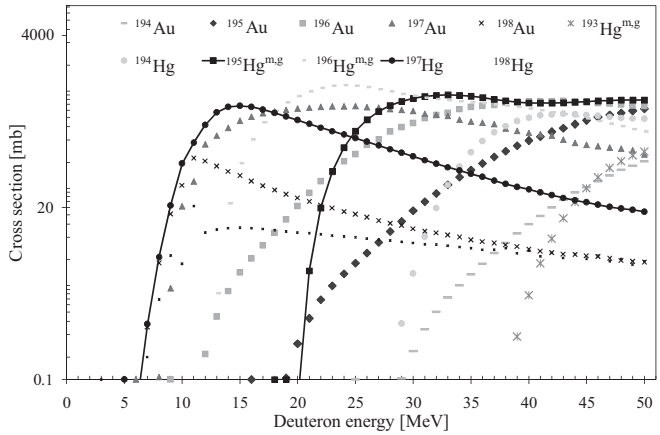

FIG. 5. TALYS-1.26 calculated excitation function of the ^{197}Au(d,x) reaction and the impurities produced from this reaction.

separated by chemical methods. The ^{197}Au(d,4n) ^{195}Hg^{m,g} process is not appropriate to obtain unpolluted ^{195}Hg^{m,g}.

2. *Excitation function of the* ^{197}Au(d,2n)^{197}Hg^{m,g} *reaction*

Figure 6(a) shows that the ^{197}Hg production begins at about 4 MeV, and at 15 MeV, the excitation function from TALYS-1.26 reaches the maximum cross section value of 455 mb. This reaction leads to the formation of nonisotopic contaminations and mercury isotopic contamination in the 9–24-MeV energy range. To avoid the stable ^{196}Hg impurity and to attain the full benefit energy, the 9–13-MeV energy range is considered in Table I. However, stable ^{196}Hg impurity still exists in the 9–13-MeV range, and the ^{196}Hg cross section is negligible (less than 10 mb).

In this case, the cross sections are studied using different default OMPs in TALYS and the optical model parameters from Daehnick *et al*. [35], Bojowald *et al*. [36], Han *et al*. [37], and An *et al*. [38]. Figure 6(a) shows the TALYS-1.26 calculations by the default OMPs, which are significantly close to the experimental isomeric cross sections [47] as compared to other OMP calculations. Furthermore, TENDL overestimates the isomeric cross sections values. For the ground-state cross section, up to 11 MeV, EMPIRE-3 agrees reasonably well with the experimental data. However, Fig. 6(c) shows that above 9 MeV, the calculations based on the Bojowald *et al*. [36], Han *et al*. [37], and An *et al*. [38] OMPs agree with the experimental measurements noticeably better than TALYS in the default mode. In fact, the TALYS-1.26 calculation based on the default OMPs underestimates the values, and TENLD unexpectedly overestimates the values. According to the SRIM code, the required target thickness should be 77.3 μm of gold. The calculated production yields are shown in Table I.

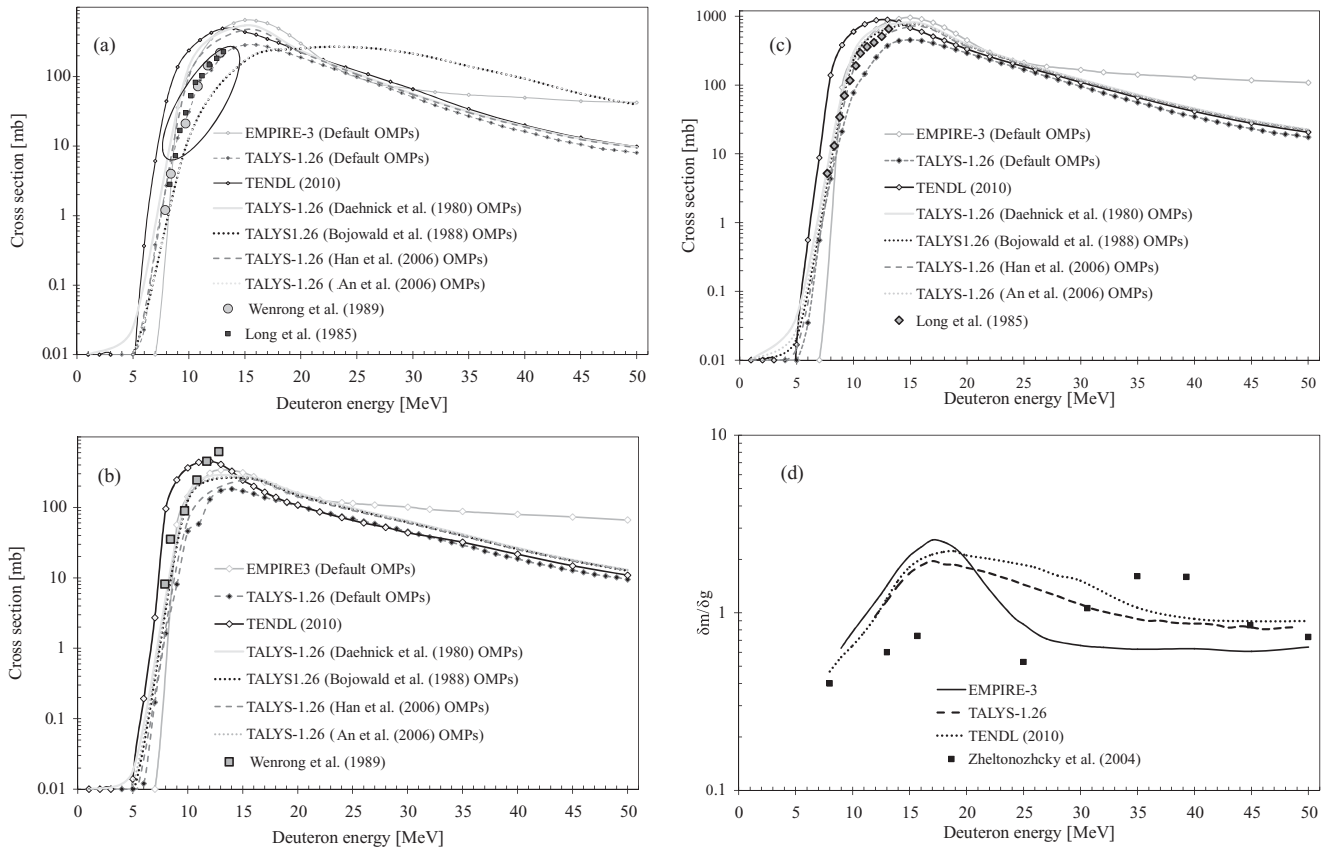

FIG. 6. Comparison between the experimental cross section data and the calculated excitation functions by TALYS-1.26, TENDL, and EMPIRE-3 for the ^{197}Au(d,2n)^{197}Hg^{m,g} reaction. (a) total production cross section, (b) isomer-state population, (c) ground-state population, and (d) isomer ratio in the ^{197}Au(d,2n)^{197}Hg^{m,g} process. The experimental data are from Refs. [50–52].

TABLE II. Nuclear characteristics and applications of mercury radioisotopes.

Radionuclide	$T_{1/2}$ (h)	Decay mode	γ (keV)	E_{Av}, all light particles (keV)	E_{Av}, all electromagnetic radiations (keV)	Proposed application
^{192}Hg	4.85	β^+, EC	274.9 (50.4%)	52.671	271.411	Medicinal and *in vivo* application [7]
^{193}Hg^m	11.8	β^+, EC, IT	258.1 (60%), 407.9 (25%), 573.5 (14.2%)	768.435	778.573	Medicinal and *in vivo* application [7]
^{193}Hg	3.8	β^+, EC		781.122	781.122	Medicinal and *in vivo* application [7]
^{195}Hg^m	41.52	β^+, EC, IT	261.7 (31%), 560.3 (7%)	266.572	362.019	Vascular imaging [55]
^{195}Hg^g	9.9	β^+, EC	585.1 (1.9%), 779.8 (6.8%)	52.611	193.376	
^{197}Hg^m	23.8	β^+, EC, IT	133.9 (34%), 279.0 (5%)	25.772	298.966	Nuclear imaging and therapy [2]
^{197}Hg^g	64.14	β^+, EC		200.037	200.037	Radiotracer [2], nuclear imaging and therapy [2]
^{199}Hg^m	0.71	IT	158.3 (52.3%), 74.1 (13.5%)		532	Nuclear imaging [7]
^{203}Hg	1118.16	β^-	279.2 (81.5%)	107.807	240.34	Radiotracer [7,10,56], biodistribution [8,9]

IV. DISCUSSION

In Fig. 4(a), at 20–25 MeV, there is a gap in the experimental data. Because EMPIRE-3 agrees well with the experimental data at about 19 MeV and higher than 25 MeV, the EMPIRE-3 calculations in the 20–25-MeV range could be acceptable values. Moreover, the isomer ratio in the ^{197}Au(p,2n)^{197}Hg^{m,g} process [Fig. 4(d)] indicates that the EMPIRE-3 data at about 20 MeV are in good agreement with the experimental measurements.

Evidently, the ^{197}Au(d,2n)^{197}Hg^m reaction demonstrated a significant improvement in the results of TALYS-1.26 against TENDL [this improvement has been circled in Fig. 6(a)]. Additionally, TALYS-1.26 and TENDL had similar results in most other reactions.

Regarding our results, it was unnecessary to change the OMPs in our calculations except for the ^{197}Au(d,2n)^{197}Hg^{m,g} total production cross sections. In this case, the Bojowald *et al.* [36], Han *et al.* [37], and An *et al.* [38] OMPs seem more reasonable to calculate the total production cross sections.

For certain isotopes, there could be an advantage to a certain production method [52–54]. Overall, to produce ^{197}Hg^{m,g}, the ^{197}Au(d,x) reaction process was determined to be more interesting than the ^{197}Au(p,x) reaction due to its slightly higher yield and considerably smaller target thickness. In addition, from the calculation of the TALYS-1.26 excitation function of the ^{nat}Pt(α,x) reaction and the impurities produced from this reaction, we evaluate the production of ^{195}Hg^{m,g} and ^{197}Hg^{m,g} and find that in the ^{nat}Pt(α,x) reaction, the stable ^{196}Hg impurity prevents the production of unpolluted radionuclides. Table II briefly demonstrates the nuclear characteristics and the proposed application of various mercury radioisotopes.

V. CONCLUSIONS

In this paper, the production methods and the applications of mercury radionuclides were briefly outlined. The possibility of the cyclotron production of ^{195}Hg^{m,g} and ^{197}Hg^{m,g} was evaluated in detail. TALYS-1.26 and EMPIRE-3 nuclear model calculation codes were used to evaluate the cross sections of the mercury radionuclides. These codes were able to calculate the excitation functions for the residual nuclide production, including the isomeric cross sections that are indispensable in calculating the excitation function of the mercury reactions. Moreover, we employed four sets of optical model parameters beside the defaults of the TALYS code. Consequently, we compared the calculations with the reported experimental measurement. The ^{195}Hg^{m,g} and ^{197}Hg^{m,g} production yield was calculated in regard to the excitation function calculations and the stopping powers of the projectiles in gold. The thickness of the targets was obtained using the SRIM code for each reaction. To produce ^{195}Hg^{m,g} and ^{197}Hg^{m,g}, the ^{197}Au(d,2n)^{197}Hg^{m,g} and ^{197}Au(p,3n)^{195}Hg^{m,g} reactions were determined to be the most interesting candidates.

The first three authors (M.S., M.B., and M.K.B.) performed the research. M.S. developed the design and concept of the study; M.B. investigated the nuclear model calculations and the nuclear codes; and M.K.B. analyzed the data and prepared the manuscript. A.M. and M.L. were responsible for literature search.

ACKNOWLEDGMENTS

The authors wish to express their thanks to Dr. Arjan Koning of the Nuclear Research and Consultancy Group, Petten, Netherlands, for providing the most up-to-date versions of TALYS and for invaluable help and discussions. Additionally, the authors would particularly like to thank Mr. Morteza Aref of the Physics Faculty, University of Zanjan, Zanjan, Iran, for his technical support in the Linux-based software aspects of this work. Last, the authors would like to express their sincere thanks to Dr. Roberto Capote Noy of IAEA Nuclear Data Section, Vienna, Austria, for his useful advice on application of the EMPIRE code.

[1] M. K. Bakht and M. Sadeghi, Ann. Nucl. Med. **25**, 529 (2011).
[2] M. K. Bakht, M. Sadeghi, and C. Tenreiro, J. Radioanal, Nucl. Chem., doi: 10.1007/s10967-011-1483-2.
[3] M. Sadeghi, N. Zandi, and M. Bakhtiari, J. Radioanal, Nucl. Chem. doi: 10.1007/s10967-011-1557-1.
[4] M. Sadeghi, M. Enferadi, and M. Bakhtiari, Ann. Nucl. Energy. **41**, 97 (2012).
[5] M. Neves, A. Kling, and A. Oliveira1, J. Radioanal. Nucl. Chem. **266**, 377 (2005).
[6] E. K. Elmaghraby, K. F. Hassan, H. Omara, and Z. A. Saleh, Appl. Radiat. Isot. **68**, 1694 (2010).
[7] S. Lahiri, K. Banerjee, and N. R. Das, J. Radioanal. Nucl. Chem. **242**, 497 (1999).
[8] M. A. Morcillo and J. Santamaria, Biometals **4**, 301 (1995).
[9] M. J. Vimy, Y. Takahashi, and F. L. Lorscheider, Am. J. Physiol. **258**, 939 (1990).
[10] K. J. Tuli, *Nuclear Wallet Cards (National Brookhaven Laboratory*, Upton, NY, 2005).
[11] S. R. Guevara, S. Žižek, U. Repinc, S. P. Catán, R. Jaćimović, and M. Horvat, Anal. Bioanal. Chem. **387**, 2185 (2007).
[12] G. R. Choppin, J. O. Liljenzin, and J. Rydberg, *Radiochemistry and Nuclear Chemistry*, 3rd ed. (Butterwort-Heinemann, Oxford, 2002).
[13] S. M. Qaim, Radiochim. Acta. **89**, 223 (2001).
[14] E. M. Mokrzan, L. E. Kerper, and N. Ballatori, J. Pharmacol. Exp. Ther. **272**, 1277 (1995).
[15] K. Gul, Nucl. Instrum. Methods Phys. Res., Sect. B **269**, 764 (2011).
[16] M. Herman, P. Obložinský, R. Capote, M. Sin, A. Trkov, A. Ventura, and V. Zerkin, in *Proceedings of International Conference on Nuclear Data for Science and Technology*, AIP Conf. Proc. No. **769** (AIP, New York, 2005), pp. 1184–1187.
[17] J. Raynal, CEA Saclay, Report No. CEA-N-2772, 1994 (unpublished).
[18] T. Belgya *et al*., IAEA, Rep. IAEA-TECDOC–1506, 2006 (unpublished).
[19] T. Tamura, T. Udagawa, and H. Lenske, Phys. Rev. C **26**, 379 (1982).
[20] H. Nishioka, J. J. M. Verbaarschot, H. A. Weidenmüller, and S. Yoshida, Ann. Phys. (NY) **172**, 67 (1986).
[21] M. Herman, A. Hoering, and G. Reffo, Phys. Rev. C **46**, 2493 (1992).
[22] E. Betàk and P. Obložinský, IAEA/Slovak Academy of Sciences, Technical Report INDC(SLK)-001, 1993 (unpublished).
[23] H. M. Hofmann, J. Richert, J. W. Tepel, and H. A. Weidenmüller, Ann. Phys. (NY) **90**, 403 (1975).
[24] D. M. Brink, Nucl. Phys. **4**, 215 (1957).
[25] P. Axel, Phys. Rev. **126**, 671 (1962).
[26] A. J. Koning, S. Hilaire, and M. Duijvestijn, TALYS-1.2, a nuclear reaction program, Nuclear Research and Consultancy Group, Petten, Netherlands, 2009 [http://www.talys.eu/].
[27] A. J. Koning and J. P. Delaroche, Nucl. Phys. A **713**, 231 (2003).
[28] M. Maiti and S. Lahiri, Phys. Rev. C **79**, 024611 (2009).
[29] S. Watanabe, Nucl. Phys. **8**, 484 (1958).
[30] A. Gilbert and A. G. W. Cameron, Can. J. Phys. **43**, 1446 (1965).
[31] W. Dilg, W. Schantl, H. Vonach, and M. Uhl, Nucl. Phys. A **217**, 269 (1973).
[32] W. Hauser and H. Feshbach, Phys. Rev. C **87**, 366 (1952).
[33] C. Kalbach, Phys. Rev. C **71**, 034606 (2005).
[34] A. J. Koning and D. Rochman, TENDL-2010: TALYS-based Evaluated Nuclear Data Library, Nuclear Research and Consultancy Group, Petten, Netherlands [http://www.talys.eu/tendl-2010].
[35] W. W. Daehnick, J. D. Childs, and Z. Vrcelj, Phys. Rev. C **21**, 2253 (1980).
[36] J. Bojowald, H. Machner, H. Nann, W. Oelert, M. Rogge, and P. Turek, Phys. Rev. C **38**, 1153 (1988).
[37] Y. Han, Y. Shi, and Q. Shen, Phys. Rev. C **74**, 044615 (2006).
[38] H. An and C. Cai, Phys. Rev. C **73**, 054605 (2006).
[39] J. F. Ziegler, M. D. Ziegler, and J. P. Biersack, Nucl. Instrum. Methods Phys. Res., Sect. B **268**, 1818 (2010).
[40] Y. Nagame, K. Sueki, S. Baba, and H. Nakahara, Phys. Rev. C **41**, 889 (1990).
[41] R. Michel, R. Bodemann, H. Busemann, R. Daunke, M. Gloris, and H. J. Lange *et al*., Nucl. Instrum. Methods Phys. Res., Sect. B **129**, 153 (1997).
[42] F. Szelecsenyi, G. F. Steyn, Z. Kovacs, and T. N. V. D. Walt, Conf. Nucl. Data Sci. Technol. **2**, 1259 (2007).
[43] M. Gusakow, Y. Legoux, and H. Sergolle, Comptes Rendus, Ser. B, Physique **251**, 70 (1960).
[44] L. F. Hansen, R. C. Jopson, H. Mark, and C. D. Swift, Nucl. Phys. **30**, 389 (1962).
[45] V. T. Gritsyna, A. P. Klyucharev, V. V. Remaev, and L. N. Reshetova, Sov. Phys. JETP **17**, 1186 (1963).
[46] F. Szelecsenyi, S. Takacs, A. Fenyvesi, Z. Szucs, F. Tarkanyi, S. J. Heselius, and J. E. Boothe, Conf. Nucl. Data. Sci. Technol. **2**, 1483-X (1997).
[47] R. G. Thomas and W. Bartolini, Phys. Rev. **159**, 1022 (1967).
[48] G. Chodil, R. C. Jopson, H. Mark, C. D. Swift, R. G. Thomas, and M. K. Yates, Nucl. Phys. A **93**, 648 (1967).
[49] S. Sudar and S. M. Qaim, Phys. Rev. C **73**, 034613 (2006).
[50] Z. Wenrong and L. Hanlin, Chin. J. Nucl. Phys. **11**, 83 (1989).
[51] X. Long, X. Peng, and F. He, Institute of Nuclear Science and Technology, Sichuan University, Report No. 001, 1985/05, 1985 (unpublished).
[52] V. A. Zheltonozhcky, V. M. Mazur, and Z. M. Bigan, Yad. Fiz. **67**, 899 (2004).
[53] A. Mushtaq, Ann. Nucl. Med. **24**, 759 (2010).
[54] M. K. Bakht and M. Sadeghi, J. Radioanal. Nucl. Chem. **288**, 937 (2011).
[55] C. Brihaye, M. Guillaume, N. Lavi, and M. Cognea, J. Nucl. Med. **23**, 1114 (1982).
[56] D. Ø. Eriksen, L. A. Tokheim, T. A. Eriksen, J. C. Meyer, and C. Qvenild, J. Radioanal. Nucl. Chem. **273**, 739 (2007).